THE ASTROPHYSICAL JOURNAL, 288:148–158, 1985 January 1

THE EFFECT OF A WEAK SHOCK ON INTERSTELLAR GAS TOWARD THE ρ OPHIUCHI CLOUD

KARIE A. MEYERS AND THEODORE P. SNOW
Laboratory for Atmospheric and Space Physics, University of Colorado

AND

S. R. FEDERMAN AND M. BREGER
Department of Astronomy, University of Texas
Received 1982 April 26; accepted 1984 July 23

ABSTRACT

We have studied the effect of a low-velocity shock on depletion in interstellar clouds. High-resolution *Copernicus* observations of interstellar absorption lines toward four stars in the ρ Ophiuchi cloud complex were used to measure differential depletion in interstellar clouds separated by velocities of 10–15 km s^{-1}. Optical observations of CH and CH^+ were used as indicators of shock strength and direction of propagation. Our observations indicate the presence of a shock with velocity ~ 10 km s^{-1} expanding away from the Sun into the ρ Oph cloud. The existence of this shock is supported by other observations quoted in the literature. We have found two distinct regions in the lines of sight. A low-density, less depleted, predominantly atomic region is associated with preshock gas, while postshock gas accounts for a predominantly molecular, more highly depleted region. Apparently a weak shock, such as the one discussed here, has the effect of enhancing grain formation or grain growth as a result of increased density in the postshock gas. It is possible for grain growth by accretion to occur in the shocked gas on time scales short compared with the cloud-crossing time of the shock.

Subject headings: interstellar: abundances — interstellar: matter — line profiles — shock waves — ultraviolet: spectra

I. INTRODUCTION

Depletion of heavy elements in varying amounts from the gas phase of interstellar clouds is a pervasive characteristic of the interstellar medium. The depleted material is thought to exist in the form of interstellar grains. Elemental variation in depletion may be a result of formation mechanisms in which some elements are preferentially condensed into grains because of their higher condensation temperatures (see Field 1974), or certain elements may be more likely to stick to grains in gas-grain collisions, as proposed by Snow (1975). If the latter scenario is more accurate, depletion should be a function of cloud density. Overall depletion is also observed to vary with respect to cloud velocity, with high-velocity clouds having little or no depletion (Routly and Spitzer 1952; Spitzer 1976; Shull, York, and Hobbs 1977; Snow and Meyers 1979). It is likely that, in these high-velocity clouds, the energetic mechanism responsible for accelerating the cloud, most likely a shock wave, is also responsible for total or partial grain destruction. Several mechanisms have been suggested to account for grain destruction, including sputtering through gas-grain or grain-grain collisions and evaporation in high-temperature post-shock gas (Barlow and Silk 1977; Cowie 1978; Shull 1978; Draine and Salpeter 1979; Havnes 1980; Seab and Shull 1983).

We have studied the effect of a low-velocity shock on the depletion in the ρ Ophiuchi cloud complex. Using high-resolution *Copernicus* observations of interstellar absorption lines toward four stars in the ρ Oph complex, we have measured depletions in clouds separated in velocity by 10–15 km s^{-1} in each line of sight. In order to confirm the presence and direction of propagation of a shock wave in the region, we have made optical observations of CH and CH^+. CH^+ is thought to be formed just behind a shock front under certain conditions (Elitzur and Watson 1978, 1980; Federman 1982*b*), and we have used the velocity shift between the CH and CH^+ lines to determine the velocity of the shock. The direction of the shock is determined by the sense of the CH/CH^+ shift. In order to obtain information about grain size and alignment, we have also measured values of λ_{max}, the wavelength of maximum polarization toward the ρ Oph stars.

In the next section we outline recent observations of the ρ Oph cloud complex. In § III, we present our observations and results, which are discussed in § IV.

II. PREVIOUS OBSERVATIONS

The Scorpius-Ophiuchus region of the sky contains many young stars and areas of recent and ongoing star formation (see, e.g., Herbst and Warner 1981). The Sco OB2 association, containing the ρ Oph stars, is a group of young stars located at a distance of 170 pc and covering an area of the sky from $l = 341°$ to $l = 2°$ and $b = +10°$ to $b = +30°$.

Many of the stars in the ρ Oph complex were observed in the high-resolution absorption-line surveys of Hobbs (1969, 1971) in Na I, Marschall and Hobbs (1972) in Ca II, and Stokes and Hobbs (1976) in Ti II. Hobbs (1971) also observed 21 cm emission toward the ρ Oph stars and was able to separate each line of sight into several velocity components. In most cases, velocities of H I and Na I components agree quite well, and Hobbs (1971) was able to derive component column densities for these elements. (If the component velocities do not agree, it is an indication that part of the H I emission originates behind the star rather than in the line of sight.) We have used velocities and column densities measured by Hobbs (1969, 1971) in our depletion determinations.

Several observers have attempted to correlate grain size with

gas density in the ρ Oph cloud. Carrasco, Strom, and Strom (1973) concluded that there are large density variations within the complex, and they found evidence that larger grains, indicated by larger-than-average values of λ_{max}, are associated with regions of higher density. Snow and Jenkins (1980) made a detailed study of density variations in the ρ Oph cloud and attempted to find a correlation between density and total line-of-sight depletion. Their observations were most consistent with a cloud composed of two regions: a dense core containing most of the atomic hydrogen as well as the CO column density, and an outer region where first ions of refractory elements exist. According to this model, refractory elements in the core do not contribute to observed UV absorption lines, either because the elements are too depleted or because the core velocity dispersion is small so that the lines from the core region are masked. Further support of the idea that there are two distinct regions may be found in Liszt (1981). He points out that when $N(H_2) = (1\text{–}40) \times 10^{19}$ cm^{-2}, true for all of the stars discussed in this paper, the column density of C I correlates best with $N(H_2)$ rather than the total hydrogen column density, while N(C II) appears to be correlated with N(H I). Federman (1981) also found a correlation between N(C I) and $N(H_2)$ in lines of sight with $N(H_2) > 10^{19}$ cm^{-2}. The implication is that the carbon ionization states delineate two separate regions in which hydrogen is nearly completely molecular or completely atomic. Crutcher (1976) has made a detailed study of the line of sight toward σ Sco and found that it is best described by a cold molecular cloud in front of an extended atomic region.

Bronfman (1980) has observed CO emission over the area of the Sco OB2 association. He finds that CO generally appears in a single broad velocity component, but can be divided into two regions. A southern cloud in the area of ρ Oph and σ Sco has CO emission between 0 and 5 km s^{-1}. (All velocities are with respect to the local standard of rest unless otherwise noted.) The northern cloud, which includes the lines of sight to β^1, ω^1, and ν Sco, shows emission between -1 and $+2$ km s^{-1}. An excellent representation of ρ Oph and the surrounding area may be found in Herbst and Warner (1981).

Our observations support the idea that there are two separate regions in the ρ Oph cloud, as in Snow and Jenkins (1980) and Crutcher (1976). However, we will postulate that the denser region, containing H_2 and CO and possibly larger grains, is the result of a low-velocity shock wave, with the less dense region consisting of preshock gas. Evidence for such a shock, both from this work and from the literature, is discussed in later sections.

III. OBSERVATIONS AND RESULTS

Basic data for the ρ Oph stars are given in Table 1, along with the lines observed toward each star in this work. The §§ III*a*–III*c* describe, respectively, the UV atomic-line observations, the optical molecular-line observations, and the polarization measurements. We have adopted Bronfman's (1980) division of the ρ Oph are into a northern and a southern cloud as described above.

a) UV Absorption-Line Observations

Copernicus observations of absorption lines were used to determine differential depletions along the lines of sight to β^1, ω^1, σ, and 1 Sco. The *Copernicus* satellite is described by Rogerson *et al.* (1973). The data used here were obtained as part of a major interstellar line survey recently completed (Bohlin *et al.* 1983). The observations were made with the U1 photomultiplier, with nominal resolution 0.05 Å. Between 2 and 10 scans were made of each line, depending on the strength of the line and the count rate. Charged-particle backgrounds were removed by standard Princeton procedures (York and Miller 1974), and scattered light levels were determined from the background counts in strongly saturated lines.

Each absorption line observed shows one or more velocity components, i.e., components separated in velocity space. Different components are assumed to correspond to different interstellar "clouds" or to different regions of the same interstellar cloud. The number and positions of velocity components for each line were determined from Hobbs's (1969, 1971) analyses. A profile-fitting program, written by A. Vidal-Madjar and C. Laurent and modified by W. Morton and D. G. York, was used to determine the best-fit parameters for each component. The program calculates a Voigt profile for each line; given the b-value and wavelength of each component, it iterates to find the combination of column densities that gives the best fit to the observed line profile. A grid of b-values, with each component b-value varying between 1.0 and 7.0, was run for each line. The final column densities were determined by the quality of the theoretical fit to the observations and by the internal agreement between column densities of lines of the same element. In general, agreement between two lines of the

TABLE 1

DATA FOR THE STARS OBSERVED

Name	HD	l	b	Spectral Type	V (mag)	$E(B-V)$ (mag)	d (pc)	Lines Observed
β^1 Sco	144217	353°11′	23°37′	B0.5 V	2.63	0.20	161	Fe II λλ1096, 1121, 1133; P II λλ1152, 1301; Mg II λ1240; Mn II λλ1197, 1201; CH λ4300; CH^+ λ4232
ω^1 Sco	144470	352 45	22 47	B2 V	4.78	0.22	227	Fe II λλ1096, 1121, 1133; P II λλ1152, 1301; Mg II λ1240; Mn II λλ1197, 1201; CH λ4300; CH^+ λ4232; λ_{max}
σ Sco	147165	351 19	17 01	B2 III	2.9	0.40	142	Fe II λλ1096, 1121, 1133; P II λλ1152, 1301; Mg II λ1240; Mn II λλ1197, 1201; CH λ4300; CH^+ λ4232
1 Sco	141637	346 06	21 43	B1.5 Vn	4.68	0.20	232	Fe II λλ1096, 1121, 1133
ν Sco	145502	354 36	22 43	B2 IVp	4.01	0.27	174	CH λ4300; CH^+ λ4232; λ_{max}

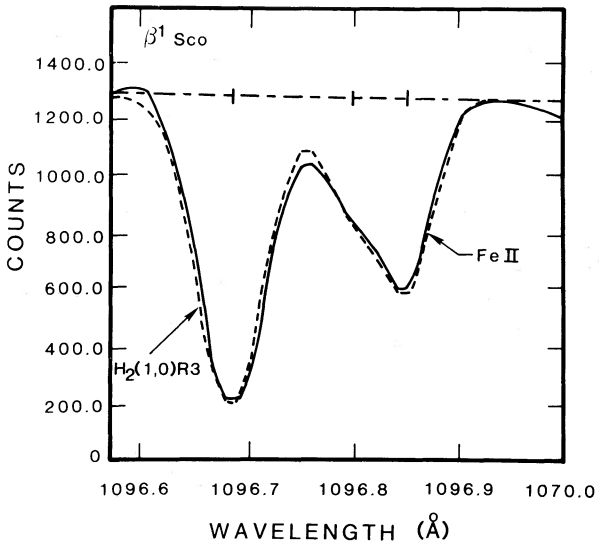

FIG. 1a

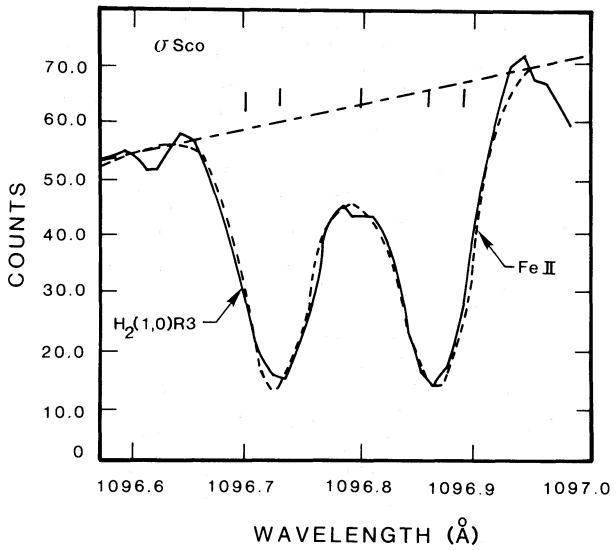

Fig. 1b

FIG. 1.—(*a*) Ultraviolet interstellar line profile toward β^1 Sco. The solid line is the observed profile. The dashed line is the best fit from the profile-fitting program. Each tick mark on the broken horizontal (continuum) line represents the central wavelength of a single velocity component. The Fe II line shown has a rest wavelength of 1096.886 Å; it is partially blended with an H_2 line at 1096.725 Å. Note that the H_2 line is apparently symmetric with a single component at the wavelength corresponding to the velocity of the more redshifted iron component. (*b*) Ultraviolet interstellar line profile toward σ Sco. The column density of the more blueshifted H_2 component is less than that of the less blueshifted component by a factor of 10^3. The center velocity component shown is from Fe II at a velocity of -20 km s^{-1} (LSR). It may be due to local gas.

same element of 50% or better in column density, and fits within a 1 σ noise level, were considered acceptable. Acceptable fits occurred for most lines only within a small range of *b*-values. Two sample absorption lines, with the adopted theoretical profiles superposed, are shown in Figure 1.

Temperature changes in the spectrometer are known to cause relative shifts in the measured wavelength scale. Wavelength scales were calibrated by assuming that the velocity of the largest component in each UV profile is the same as the velocity of the largest H I component observed by Hobbs (1971). The central point of the line width at half-maximum for the largest velocity component, as determined from the unblended half of the profile, was assumed to represent the velocity of the largest component determined by Hobbs. While this solution is not valid if there are low-column-density components which may be seen only in lines with large *f*-values, a number of checks confirm that the wavelength scale is correct. Several H_2 lines, which show contributions only from the largest velocity component with secondary components at or below noise level, were observed. The positions of the H_2 lines confirm the wavelength scale at the blue end of the observed spectral range. Using the H_2 lines to determine an initial offset of the wavelength scale, the variable offset due to temperature changes is then observed to be a small, nonrandom effect, i.e., constant over large wavelength regions. The amount of the initial offset ranged between 0 (for σ Sco and ω^1 Sco) and 5 (for β^1 Sco) km s^{-1} for the four lines of sight, while the temperature-induced variations were of the order of 3 km s^{-1}. The initial offsets in the wavelength scales are well determined, and the temperature-induced variations are smaller than the separation of velocity components.

Relative positions of the velocity components in each line, as determined by Hobbs (1971), were checked by varying the velocities of the smaller components. In most of the lines, the column densities of the smaller components were found to be insensitive to small variations (≤ 3 km s^{-1}) in the velocity separation of the two components. Larger variations in the velocity separations led to poor line fits. Thus the relative velocities are determined to within 3 km s^{-1}.

Table 2 lists the atomic data used for the UV lines observed, taken from Morton (1978). The derived column densities and *b*-values for the elements observed are given in Table 3. Upper and lower limits on *N* reflect the quality of internal agreement between lines of the same element; limits on *b* represent the range within which acceptable agreement between lines occurred.

For the Mg II observations, only one line at 1240.395 Å was available for analysis. Column densities were derived for this element by adopting the *b*-values derived for the Mn II lines. In all cases, the adopted *b*-values gave a good fit to the Mg II observations. In two of the stars, β^1 and σ Sco, there were

TABLE 2

ULTRAVIOLET ABSORPTION-LINE PARAMETERS

Ion	λ_{LAB} (Å)	Multiplet No.	g_l	g_u	γ(s^{-1})	f
Fe II	1096.886	18	10	8	3.40×10^8	0.037
	1121.987	12	10	8	3×10^{8a}	0.020
	1133.678	11	10	8	3×10^{8a}	0.0063
Mn II	1197.184	3	7	9	3.5×10^8	0.096
	1201.118	3	7	5	3.5×10^8	0.058
P II	1152.81	3	1	3	9.31×10^8	0.236
	1301.87	2	1	3	6.73×10^7	0.0173
Mg II	1240.395	...	2	2	5.45×10^7	0.000484

[a] This value of the natural damping constant is a crude estimate adopted for the profile calculations, which are insensitive to γ when the lines are as weak as those analyzed in this study, and should not be used for any other purposes.

TABLE 3

COLUMN DENSITIES AND *b*-VALUES

STAR	VELOCITY COMPONENT (km s^{-1} LSR)	log N (cm^{-2}) Fe II	Mn II	Mg II[a]	P II[a]	Ca II[b]	Ti II[b]	H I[c]	H_2[d]
β^1 Sco	+1.7	14.59 ± 0.08 (2.7 ± 1.0)	13.63 ± 0.17 (2.7 ± 1.0)	15.61 (2.7)	14.15 (2.7)	11.71	10.83	20.92	19.83
	−11.4	13.96 ± 0.12 (5.0 ± 3.0)	12.75 ± 0.09 (5.0 ± 3.0)	14.88 (5.0)	13.38 (5.0)	10.61	10.71	19.89	...
ω^1 Sco	−2.5	14.81 ± 0.17 (3.0 ± 2.0)	13.72 ± 0.05 (3.0 ± 1.0)	15.81 (3.0)	14.32 (3.0)	11.53	11.10	20.97	20.04
	−12.9	14.23 ± 0.38 (1.3 ± 0.7)	< 12.70	< 14.70	13.32 (1.3)	10.94	11.10	19.98	...
σ Sco	+4.4	15.08 ± 0.30 ($1.0^{+1.5}_{-0.5}$)	13.74 ± 0.05 (4.0 ± 1.0)	15.76 (4.0)	14.08 (4.0)	11.84	11.46	21.26	19.79
	−5.4	14.79 ± 0.05 (4.0 ± 1.0)	13.15 ± 0.11 (3.0 ± 1.0)	14.26 (3.0)	13.48 (3.0)	10.80	10.63	20.11	...
1 Sco	+3	14.30 ± 0.22 (2.6 ± 1.0)	...	...	...	...	...	20.77	19.23
	−3, −6	14.34 ± 0.24 (7.0 ± 2.0)	...	...	...	...	...	20.55	...

NOTE.—Numbers in parentheses are *b*-values.

[a] No error limits are given for the Mg II and P II values because the column densities were derived from only one line (see text). Error limits should be approximately the same (by percentage) as the corresponding Mn II error limits.

[b] Ca II and Ti II column densities are from Stokes 1978.

[c] H I column densities are from Hobbs 1971, except in the case of σ Sco. Determination of H I column densities for σ Sco is discussed in the text.

[d] H_2 column densities are from Savage *et al.* 1977. All H_2 in each line of sight is assumed to be in the more redshifted components.

discrepancies between the column densities of the two P II lines ($\lambda\lambda$1152, 1301) for any reasonable fit to the data. Column densities derived for the P II λ1152 line were in general larger than those found for the P II λ1301 line by factors of about 10. This problem also occurred in an earlier analysis of ρ Oph (Snow and Meyers 1979), and may indicate a problem with one or both P II f-values. Shull and York (1977) noted that the f-values for the P II lines are uncertain; they suggest that the correct f-values for both lines probably lie somewhere between the values given by Morton and Smith (1973) and the revised values used by Morton (1978). Our data indicate that the correction to the f-values should be made in the opposite sense, that is, the ratio f_{1152}/f_{1301} should be increased from the value used by Morton (1978). Column densities given in Table 3 for the phosphorus ion were determined using the P II λ1301 line only, since the weaker line is less affected by the choice of b-values. We used b-values derived from the Mn II lines to fit the P II λ1301 line. The P II column densities are more uncertain than those of Fe II and Mn II because of the difficulties discussed above.

i) *Depletions*

We have calculated the quantity $\zeta = \log (N/N_H)_* - \log (N/N_H)_\odot$, where the values of $(N/N_H)_\odot$ are cosmic abundances from Withbroe (1971). Here $N_H = N(\text{H I}) + 2N(H_2)$. Interstellar column densities N(H I) for each separate component were taken from Hobbs (1971). Hobbs's values were derived using 21 cm observations and include only lines of sight where the 21 cm observations are not likely to be contaminated by gas from behind the star. That the emission arises from gas in front of the stars is confirmed by a comparison of the emission data with the Lyα absorption measurements of Savage *et al.* (1977). The Lyα values for the total line-of-sight column densities toward β^1, ω^1, and 1 Sco are $(12.4 \pm 1.2) \times 10^{20}$ cm^{-2}, $(15.0 \pm 3.0) \times 10^{20}$ cm^{-2}, and $(15.5 \pm 3.1) \times 10^{20}$ cm^{-2}. Total column densities of the emission components measured by Hobbs (1971) are 9.18×10^{20} cm^{-2}, 10.4×10^{20} cm^{-2}, and 9.5×10^{20} cm^{-2} for the same lines of sight.

Hobbs (1971) did not observe the 21 cm line toward σ Sco. To find depletions in σ Sco, we used high-resolution observations of the Na I D line (Hobbs 1969), assuming the ratio of N(Na I) to N(H I) to be constant toward the Scorpius stars. Using Hobbs's (1969, 1971) values, $\log [N(\text{H I})/N(\text{Na I})] = 8.65 \pm 0.14$. Our total line-of-sight column density for H I derived from N(Na I) is 1.9×10^{21} cm^{-2}, which agrees with the H I column density found by Bohlin, Savage, and Drake (1978) of $2.2 \pm 0.8 \times 10^{21}$ cm^{-2}.

Column densities for $N(H_2)$ were taken from Savage *et al.* (1977). The molecular hydrogen was assumed to exist only in the less blueshifted, higher column density component for each star. The H_2 rotational lines observed in the UV showed symmetric profiles which were well fitted with single-component theoretical profiles. H_2 probably does exist in the secondary components, but the column densities are down by factors of 10^2–10^3 from the main components, on the basis of noise levels in the UV data, so that H_2 does not affect depletion calculations for the secondary components.

Calculation of depletions is complicated by the fact that absorption by the ions observed here may occur in H II regions. The contribution of H II regions to the lines of sight observed here is likely to be small, however. No emission nebulosity is seen on Palomar Observatory Sky Survey red plates near the stars we have observed in the ultraviolet (Herbst and Warner 1981). An emission region is seen near ν Sco; we did not calculate depletions for this star. Savage and Bohlin (1979), in a survey of iron depletions, have observed Fe III toward four of the stars discussed in this paper in order to ascertain the probable contribution of H II regions to Fe II absorption-line mea-

TABLE 4

DEPLETIONS

STAR	VELOCITY COMPONENT (km s^{-1} LSR)	$\zeta = \log (N/N_{H_*}) - \log (N/N_{H_\odot})$					
		Fe II	Mn II	P II	Mg II	Ca II	Ti II
β^1 Sco	+1.7	−1.77	−0.63	−0.24	−0.88	−3.58	−2.87
	−11.4	−1.33	−0.34	+0.06	−0.56	−3.20	−1.65
ω^1 Sco	+2.5	−1.63	−0.52	−0.15	−0.78	−3.84	−2.68
	−12.9	−1.15	< −0.48	−0.09	< −0.82	−3.37	−1.62
σ Sco	+4.4	−1.60	−0.74	−0.63	−1.06	−3.77	−2.56
	−5.4	−0.73	−0.17	−0.07	−1.40	−3.62	−2.20
1 Sco	+3	−1.88	...	...	...	...	...
	−3, −6	−1.61	...	...	...	...	...

surements. Fe II is the dominant ion in neutral regions, while Fe II and Fe III should have similar column densities in ionized regions (Olthof and Pottasch 1975). The quantity N(Fe III), then, is an indicator of the fraction of Fe II absorption from H II regions. Savage and Bohlin (1979) find upper limits for the ratio N(Fe III)/N(Fe II) between 0.013 and 0.033 for the stars β^1, ω^1, and ν Sco, indicating that less than 5% of the Fe II absorption in these lines of sight is from H II regions.

Table 4 gives the depletion by component for each of the stars observed, along with some depletions calculated from published data as noted. Errors in the depletion determinations are between 0.1 and 0.2 in the log and are due to the 50% margin in agreement of column densities for lines of the same element. Added to this are probable but undetermined errors from the H I measuremments of Hobbs (1971) and, in the case of σ Sco, the error involved in calculating N(H I) from N(Na I). Although the errors are fairly large, there is a general trend for the less blueshifted components to be more depleted in heavy elements. As seen most clearly in the iron data, the measurements indicate that the larger, less blueshifted cloud is more depleted in each star by factors of 0.2–0.8 dex. We conclude that approximately twice as much iron has been depleted onto grains in this cloud. Manganese and phosphorus clearly show similar trends. Although the P II depletions in Table 4 are uncertain because of uncertainties in the column densities discussed above, the sense of the depletion differences between velocity components should be correct. Note that the depletions found here for P II, using the P II λ1301 line with Morton's (1978) f-value, are not inconsistent with phosphorus depletion determinations in other moderately reddened lines of sight (Snow 1975).

b) CH *and* CH$^+$ *Observations*

The measurements of CH λ4300 and CH$^+$ λ4232 were made on the coudé spectrograph of the 2.7 m telescope at McDonald Observatory. The CH and CH$^+$ observations were performed in 1981 June and 1980 June, respectively. The spectra were obtained with the Reticon photodiode array (Vogt, Tull, and Kelton 1978). The basic instrumental configuration was described by Federman (1980); one change was made for the present observations. The entrance slit of the spectrograph was set at 440 μm for the CH measurements. This setting corresponds to an instrumental resolution of 4.4 km s^{-1}, which was still sufficient to resolve the line. The CH$^+$ data were taken with the instrumentation as described by Federman (1980); the resolution was 2.2 km s^{-1}. The larger slit used in the CH observations was required to ensure that detections of 1 mÅ features were possible in a reasonable amount of time.

The data were reduced in two steps. First, a program was used which produced flat continua and which removed any fixed-pattern noise remaining after the data had been processed with the Reticon software package (Vogt, Tull, and Kelton 1978). The equivalent width W_λ of each line was determined through the use of a planimeter. The error associated with the value of W_λ was calculated from the root mean square error in the continuum. Second, the velocity at line center in the local standard of rest, v_{LSR}, and the Doppler parameter, b, were derived from a least squares program that fitted a Gaussian profile to the lines. The Doppler parameter was obtained from the fit after the contribution to the line width from the instrumental resolution had been accounted for. The errors associated with v_{LSR} and b were determined from the quality of the least squares fit.

The results of the molecular observations are displayed in Table 5. Data were obtained for the lines of sight toward β^1, ω^1, ν, and σ Sco. The first column lists the molecular feature; the remaining columns present W_λ, v_{LSR}, and b. For each of the parameters 1 σ errors are quoted. For W_λ, the error is the rms error over the full width of the line.

Hobbs (1973) measured CH$^+$ absorption toward β^1, ω^1, and σ Sco. The value for the equivalent width toward β^1 and σ Sco is 50% of the value found in the present work; within the 2 σ limits of each measurement, however, the results are consistent. The two measurements for W_λ(CH$^+$) toward ν Sco agree with

TABLE 5

RESULTS OF THE CH AND CH$^+$ MEASUREMENTS

MOLECULE	W_λ (mÅ)	v_{LSR} (km s^{-1})	b (km s^{-1})
	β^1 Sco		
CH	3.5 ± 1.3	+1.9 ± 0.7	3.3 ± 0.9
CH$^+$	3.9 ± 1.1	−0.9 ± 0.3	3.2 ± 0.5
	ω^1 Sco		
CH	3.0 ± 1.5	+1.7 ± 0.6	3.2 ± 0.7
CH$^+$	4.1 ± 1.6	−1.4 ± 0.2	2.7 ± 0.3
	ν Sco		
CH	2.8 ± 1.2	+2.5 ± 0.5	2.1 ± 0.7
CH$^+$	3.4 ± 1.4	−0.6 ± 0.4	2.7 ± 0.4
	σ Sco		
CH	3.9 ± 1.6	+3.8 ± 0.5	3.1 ± 0.6
CH$^+$	6.8 ± 2.5	+3.1 ± 0.6	2.8 ± 0.7

each other. The value for the line width is similar for each direction. The velocity of the line centers is shifted by 1.0–1.5 km s^{-1} to the red of the present velocities. Federman (1982*a*) noted this difference, but mentioned that within the uncertainties of the two measurements, the velocities are the same. The present measurements included an Fe/Ne calibration spectrum before and after each observation. The spectrograph was stable to within 1.1 km s^{-1}; Hobbs (1973) determined that his velocities are accurate to ~ 0.5 km s^{-1}.

The uncertainty in velocity does not weaken the argument for a separation in velocity between CH and CH^+ found in the present study, for the following reasons. The separation is two to three times greater than the uncertainty in the velocity of the CH^+ line. The Ca II measurements of Marschall and Hobbs (1972) toward β^1 and ω^1 Sco show atomic features, which are not strongly saturated, at the velocities deduced from the present work; in the case of β^1 Sco, an extended blue wing appears in the line centered near 2 km s^{-1}. No measurements of weak atomic lines are available for σ Sco. The shock velocity deduced from the separation in the molecular lines is consistent with the separation in velocity of the atomic ultraviolet features. This is to be expected if the separation in atomic velocities is due to the shock in which the CH^+ is formed. This point is discussed in more detail in § IV.

c) *Polarization Measurements*

Three bright stars in the Scorpius region were measured with the linear polarimeter attached to the 2.1 m telescope at McDonald Observatory. Since the previous description of the equipment and its performance (Breger 1979), a device that automatically calibrates position angles has been added. A Polaroid sheet calibrated from standard stars can be inserted into the beam. Due to the excessive brightness of these Scorpius stars at some wavelengths, some of the observations were made during cloud cover. Many tests have shown that cloud cover does not affect the accuracy of the polarization measurements, since the detecting Glan prism spins at a rapid rate of 1429 revolutions per minute. Small coincidence corrections utilizing the dead time (easily measured with a polarimeter) were applied.

Table 6 lists the measurements obtained during 1981 May 3 and 4 (UT). The filter information refers to the effective wavelengths, in microns, of the broad-band filters used. Where the measurement uncertainties were less than $\pm 0.01\%$, we have listed the higher (worst) of the estimates based on photon statistics and on the agreement between multiple observations. The measured polarization of ω^1 Sco, ν Sco Ab, and ν Sco CD fitted the standard interstellar relation by Serkowski, Mathewson, and Ford (1975, hereafter SMF). The applicable values of λ_{max} and p_{max} are also given in Table 6. For the two stars in common with SMF (ω^1 Sco, ν Sco CD), our values of λ_{max} agree to within ± 0.01 μm in both cases.

The quantity λ_{max} is the wavelength at which polarization reaches its maximum value p_{max}, and is an indicator of average grain size. Average grain size in the direction of these three stars is larger than the median interstellar value of 0.545 μm found by SMF. The effect is rather small for ω^1 Sco, but becomes very large for ν Sco AB and ν Sco CD. We also note the slight rotation of position angle of polarization for all three stars, with an average value of 1°.9 from the red to the ultraviolet region. Such a rotation is confirmed by SMF for the two stars in common.

The two binaries ν Sco AB and ν Sco CD are separated by 42″, and comprise the quadruple system ν Sco. They are far enough apart to be measured independently. The interstellar medium in front of the two systems shows similar, but not identical, behavior. The effective grain size is large in both cases, as indicated by $\lambda_{max} = 0.69$ and 0.74 μm, but the two wavelength-dependence curves are not the same. The position angles of polarization differ by 5°. Table 7 summarizes the available data, where the sources are this paper and SMF.

IV. DISCUSSION

The atomic absorption data show that, of two main clouds of gas in the Sco OB2 direction, the cloud which contains most of the column density and which has an LSR velocity of -10 to -15 km s^{-1} is less depleted than the smaller, lower velocity cloud. Taken alone, the absorption-line data support the idea that higher velocity gas is less depleted than low-velocity gas. In this section, we discuss another possible interpretation of

TABLE 6

NEW POLARIZATION MEASUREMENTS

Filter (μm)	Polarization (%)	Position Angle (deg.)	λ_{max} (μm)	p_{max} (μm)	(%)
ω^1 Sco:					
0.354.....	0.874 ± 0.029	117			
0.44	1.053 ± 0.011	118			
0.54	1.133 ± 0.01	118	0.58 ± 0.02	1.14 ± 0.02	
0.65	1.106 ± 0.01	118			
0.74	1.068 ± 0.026	119			
ν Sco AB:					
0.36	0.764 ± 0.012	139			
0.44	0.973 ± 0.011	140			
0.54	1.195 ± 0.013	140	0.69 ± 0.02	1.26 ± 0.02	
0.65	1.256 ± 0.01	141			
0.74	1.235 ± 0.32	141			
ν Sco CD:					
0.354.....	0.628 ± 0.01	144			
0.44	0.827 ± 0.01	145			
0.54	0.991 ± 0.01	144	0.74 ± 0.03	1.11 ± 0.04	
0.65	1.099 ± 0.01	146			
0.74	1.102 ± 0.01	146			

TABLE 7

POLARIZATION IN THE SCORPIUS-OPHIUCHUS REGION

Star	λ_{max} (μm)	R_{av}[a]	Position Angle[b] (deg)
ω^1 Sco	0.58 ± 0.02	3.2	2
ν Sco AB	0.69 ± 0.02	3.8	2
ν Sco CD	0.74 ± 0.03	4.1	2
β^1 Sco	0.61 ± 0.02	3.4	2
σ Sco	0.56 ± 0.02	3.0	4:
ρ Oph C	0.72 ± 0.04	4.0	2
ρ Oph AB	0.68 ± 0.02	3.7	0
ζ Oph	0.59 ± 0.02	3.2	3

[a] Inferred value of the average ratio of total to selective extinction.

[b] Θ (red) minus Θ (ultraviolet).

the data, which is suggested by the observations of CH and CH^+ summarized in Table 4.

a) CH^+ Formation in Shocks

In the low-temperature interstellar medium, CH^+ is destroyed rapidly by dissociative recombination. In order to explain previously observed column densities of this species, Elitzur and Watson (1978, 1980) have postulated that CH^+ is produced in high-temperature regions immediately behind shock fronts. The reaction by which observable amounts of CH^+ may be produced,

$$C^+ + H_2 \rightarrow CH^+ + H ,$$

is endothermic by 0.4 eV, but it should take place at sufficiently high temperatures ($T > 10^3$ K). Elitzur and Watson (1978) found that the column density of CH^+ produced through this reaction reaches a maximum behind a shock of velocity $V_s =$ 12–14 km s^{-1}, contingent upon optimum preshock ambient conditions, i.e.,

$$n_H \sim 4\text{–}5 \text{ cm}^{-3}; \qquad n_{H_2}/n_H \gtrsim 0.01 .$$

In the Elitzur and Watson (1978) picture, CH^+ is formed in the adiabatic postshock region, while CH and other molecules form farther behind the shock, in the cooled, isothermal region of the shock. Thus the velocity separation between the CH and CH^+ absorption lines observed toward such a shock is one-fourth of the shock velocity, if no geometrical correction is required. (See Spitzer 1978 or Dyson and Williams 1980 for a discussion of shock structure.) From an extensive survey of CH and CH^+, Federman (1982*b*) showed that the most consistent picture for all available data requires the presence of shocks to produce CH^+.

b) The ρ Oph Cloud

Assuming that the CH^+ observed in the Sco OB2 lines of sight is formed in a shocked layer, the optical molecular data reveal the properties of the shock. The separation of the CH and CH^+ velocities given in Table 5 implies a velocity of 10–15 km s^{-1} for the shock propagating in the northern cloud of the complex, which includes the lines of sight to β^1, ω^1, and ν Sco. Furthermore, a CH line redshifted with respect to the CH^+ line indicates that the shock is expanding away from the Sun, in the sense that the postshock gas has a less negative velocity than the gas into which the shock front is expanding.

In the northern cloud, the separation of velocity components in the UV atomic absorption lines is 10–15 km s^{-1}, which agrees well with the shock velocities indicated by the CH/CH^+ velocity separations. We conclude that the atomic velocity separations are produced by the shock whose presence is inferred from the observed CH^+ column densities. The direction of shock propagation, away from the Sun toward the ρ Oph stars, leads to the conclusion that the more blueshifted atomic gas exists in the preshock gas cloud, while the redder component may be associated with postshock gas. The velocities of the redder atomic components in each line of sight agree within the errors with the observed CH velocities, supporting the conclusion that this component is associated with postshock gas.

The line of sight toward χ Oph may also pass through the northern cloud. However, this star is more than 25 pc closer to the Sun than the other stars associated with the northern cloud (Savage *et al.* 1977). Thus, the detections of a blueshifted CH line toward the star (Frisch 1979) may not refer to the gas toward β^1, ω^1, and ν Sco.

An upper limit of 2.2 km s^{-1} was obtained for the shift between the CH and CH^+ lines toward σ Sco; thus a shock velocity of $\lesssim$10 km s^{-1} is implied for the southern cloud. Other data also suggest a smaller shock velocity for the southern cloud direction. The ultraviolet lines toward σ Sco and 1 Sco have two components separated by $\sim$10 km s^{-1}, with the redder component again at the velocity of the CH feature. If the observed distribution of rotational levels in the vibrational ground state of H_2 (Spitzer, Cochran, and Hirshfield 1974) occurs through collisions behind a shock, the shock velocity must be $\lesssim$10 km s^{-1} (Elitzur and Watson 1980). (The upper limit arises because optical pumping also influences the distribution of levels.) As in the northern cloud, we have identified the redder component of the atomic absorption toward σ Sco and 1 Sco as postshock gas from a shock of velocity $\lesssim$10 km s^{-1}.

Table 4 shows that the refractory elements observed toward ρ Oph are substantially more depleted in the postshock than in the preshock gas. Previous studies of interstellar depletion (e.g., Siluk and Silk 1974; Shull, York, and Hobbs 1977) have shown correlations between cloud velocities and refractory element abundances for high-velocity clouds ($v \gtrsim 50$ km s^{-1}). High-velocity clouds are observed to have less depletion than low-velocity clouds, with the highest velocity clouds showing near-solar abundances. The clouds are generally assumed to be accelerated by strong shocks ($V_s \geq 50$ km s^{-1}); gas-grain and grain-grain collisions cause grain destruction in the shocks, so that solid material is returned to the gas-phase interstellar medium and the postshock gas is less depleted than the original unshocked gas (Shull, York, and Hobbs 1977). However, for the slow shock observed here, the postshock medium is more depleted than the unshocked gas. Apparently in a slow shock, grains are not appreciably destroyed, and grain growth is actually enhanced in the dense postshock region.

Our data, combined with previous observations discussed in § II, suggest that the ρ Oph cloud consists of two distinct regions delineated by a shock front traveling with a speed of about 10 km s^{-1}. In this scenario the shock expands into a predominantly atomic gas cloud [$N(H_2) \lesssim 0.1N(H)$]. CH^+ is formed in the hot adiabatic region just behind the shock front, and the CH^+ line is blueshifted with respect to the shock front by an amount corresponding to a velocity of $(1/4)V_s$, or 2–3 km s^{-1}. CH, as well as other molecules including H_2 and CO, is formed in the dense, cooled postshock gas; lines from these molecules occur at the shock velocity V_s. Grain growth, as

deduced from the depletion and polarization studies, takes place in this postshock region, so that gas in the postshock region is approximately twice as depleted in refractory elements as the gas in the preshock region. A schematic representation of the Sco OB2 lines of sight as deduced from our observations is shown in Figure 2. Note that this view requires that the interstellar material in the ρ Oph region have a preshock velocity of about -10 km s^{-1} with respect to local standard of rest. The shock front is then expanding away from the sun toward the Sco OB2 association, and the shocked gas is manifested in the less blueshifted velocity components.

The gas in the ρ Oph complex appears to have the same general properties in both the northern and southern clouds, except that the shock has a somewhat lower velocity toward the southern cloud. It is possible that the shock has encountered more interstellar material in this direction so that the shock front has been decelerated. This is not indicated by the column density measurements toward σ Sco, however. It is also possible that the shock is moving in a slightly different direction in the southern cloud, so that the projected velocity we observe is different. The similarities in the velocity structure of the atomic absorption profiles seem to preclude the possibility that shocks in the northern and southern clouds have two different origins (see Fig. 1).

Three molecules whose velocities have been observed appear to have single velocity components at or near the velocity of the less blueshifted atomic gas component, which we have designated postshock gas. Bronfman (1980) observed CO emission and found a single broad velocity component. The northern cloud shows CO emission between -1 and $+2$ km s^{-1}, and the southern cloud emission is between 0 and 5 km s^{-1}. The optical absorption lines of CH show velocities of about 0 km s^{-1} toward β^1 and ω^1 Sco, and 2–3 km s^{-1} toward σ Sco (Table 4). The H_2 absorption lines observed in the ultraviolet program appear to be symmetric about the velocity of the less blueshifted atomic component, as shown in Figure 1. Therefore, there is considerable evidence that nearly all of the molecular column density, with the exception of CH^+, is concentrated in a single broad velocity component near 0 km s^{-1}. This component can be identified with more depleted, postshock atomic gas.

The view of the ρ Oph cloud described above is consistent with physical conditions necessary for CH^+ to be formed behind a shock. The deduced shock velocity, 10–15 km s^{-1}, is near that required by Elitzur and Watson (1978) for maximum CH^+ formation. Measurements of the space density of hydrogen toward the ρ Oph stars using CO rotational excitation

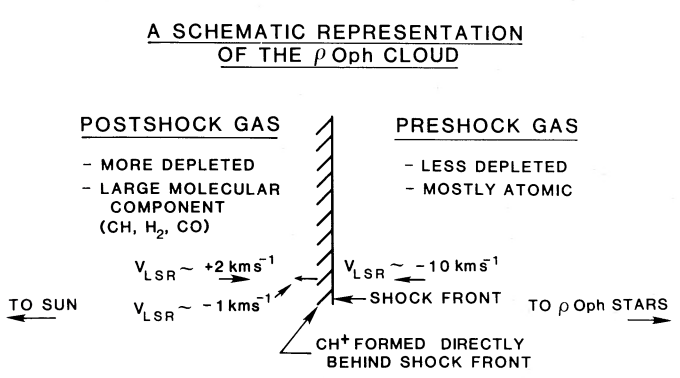

FIG. 2.—This diagram shows the distribution of the gas near the ρ Oph stars, deduced from the observations discussed in the text.

(Snow and Jenkins 1980) give values near 500 cm^{-3} for the molecular region of the cloud. If the molecules exist in the isothermal postshock gas, which is compressed by a factor of the square of the Mach number, a preshock density of $n_H \sim$ 3–5 cm^{-3} is implied, assuming that shock compression is along magnetic field lines. This is a typical space density for diffuse clouds and is consistent with the Elitzur and Watson (1978) model. The ratio n_{H_2}/n_H is uncertain in the ρ Oph cloud, but in the gas which we assume to be preshock gas the ultraviolet H_2 observations indicate that $N(H_2)/N(H\ I) \lesssim 0.1$. Given the uncertainties in the H-H_2 collisional cross sections used by Elitzur and Watson (1978) and the uncertainties in the n_{H_2}/n_H ratio in the ρ Oph cloud, a strong statement cannot be made as to whether H_2 is present in sufficient quantities in the preshock gas to produce CH^+. However, the theoretical optimum value of $n_{H_2}/n_H \gtrsim 0.01$ is not incompatible with the upper limit of $N(H_2)/N(H\ I) \lesssim 0.1$.

c) *Grain Growth in the Postshock Gas*

In considering a model in which grain growth by accretion occurs behind a shock front, it is important to consider whether grain growth of the magnitude observed can take place on a time scale small compared with the cloud-crossing time of the shock. A crude calculation of the probable rate of accretion onto grains behind the shock front may be made as follows. Since the depletion in the postshock gas increases by about a factor of 2, we will calculate the time required for a grain to increase its radius by a factor of $(2)^{1/3}$ by accretion. According to Spitzer (1978, eq. [9-29]), the rate of change in grain radius, a, is

$$\frac{da}{dt} = \frac{w_a \rho_a \xi_a}{4\rho_s},$$

where ρ_a and w_a are the mass density and velocity of the colliding atoms, ρ_s is the density of matter in the grains, and ξ_a is the sticking probability of the atom on the grain surface. Taking $T = 80$ K and $n_H = 500$ cm^{-3}, typical parameters for the dense region of the ρ Oph cloud as observed in Snow and Jenkins (1980), $da/dt = (5 \times 10^{-12}$ cm yr$^{-1})\xi_a$, or $\Delta t \approx (2 \times 10^{11})\Delta a \xi_a^{-1}$ yr with Δa in cm. For $\Delta a \sim 1.3 \times 10^{-6}$, which is a volume increase of a factor of 2 for grains with $a \sim 10^{-5}$ cm, $\Delta t \approx (3 \times 10^5$ yr$)\xi_a^{-1}$. The crossing time for a 15 km s^{-1} shock crossing a 10 pc cloud is 6×10^5 yr. For neutral atoms, ξ_a is very close to 1 (Spitzer 1978); the value of ξ_a for ions is somewhat uncertain, however, the cross section for gas-grain collisions is larger in the case of ions (assuming that the grains are negatively charged in the dense postshock region). Thus, it should be possible to observe both a more depleted postshock region and a less depleted preshock region in the same interstellar cloud.

Jura (1980) has argued that grain growth by coagulation can best explain the observed properties of the extinction curve toward ρ Oph. The total extinction per gram of material toward ρ Oph, A_V/N_H, is lower than the average interstellar value by about a factor of 2, which might be expected if grain growth occurred by coagulation rather than by accretion. In Jura's (1980) model, the large graphite grains ($a \sim 1$ μm) grow in radius by a factor of 2–3 through coagulation, so that total extinction is decreased but the long- and short-wavelength extinctions remain approximately constant; the amount of material found in grains stays constant.

Our observations indicate, however, that in the denser

portion of the ρ Oph cloud, the amount of material in the grains has increased, although probably not enough to increase grain radii by factors of 2–3. It is possible that grain growth occurs in the postshock gas through a combination of accretion and coagulation. Coagulation could account for a large increase in the radii of some of the grains and the increase in λ_{max} toward the ρ Oph clouds, while accretion would account for the depletion increase in the postshock gas and also possibly the absence of very small grains indicated by the anomalously low far-UV extinction toward σ Sco and ρ Oph (Bless and Savage 1972; Snow and York 1975; Seab, Snow, and Joseph 1981). By considering the mean path lengths for grain-grain and atom-grain collisions, we can see that small grains are more likely to grow by accreting material, while large grains grow faster by coagulation. Let λ_{dd} be the mean free path length for grain-grain collisions and λ_{dg} be the mean path length for a grain to encounter a mass of gas equal to the grain mass. The value of λ_{dd} is just $(\alpha n_H \xi_d)^{-1}$, where α is a numerical constant between 1 and 4 which takes into account a distribution of grain sizes a and the probability that a grazing-incidence collision will produce coagulation, and ξ_d is the mean dust grain cross section per H atom and is equal to 10^{-21} cm^2 (Spitzer 1978). (We have assumed that all grain velocities are small enough that evaporation due to collisions is negligible. This will occur if the grains are not accelerated much because of the weakness of the shock, or if collisions with H and He atoms in the shocked gas reduce high grain velocities [Spitzer 1978].) The mean path length for a grain to double in size by accretion, λ_{dg}, is given by

$$\lambda_{dg} = \frac{4a\rho_s}{3n_a A m_H \xi_a} = \frac{4a\rho_s}{3\rho_a \xi_a},$$

where $\rho_a = n_a A m_H$ is the mass density of accreting atoms. Thus λ_{dg} is proportional to a, the grain radius, and the ratio $\lambda_{dg}/\lambda_{dd} \propto a$. For $a = 10^{-5}$ cm, $\lambda_{dg}/\lambda_{dd} \approx 10$, so that in the time for the depletion to increase by a factor of ~ 2, most larger grains will have undergone some coagulation, but most smaller grains will have grown only slightly, by accretion. In this way, A_V/N_H would be reduced because of grains "hiding behind" the largest grains, as described in Jura (1980), and the depletion results are also explained.

d) *Geometry of the Shock*

The Sco OB2 association lies in a well-studied and active region of the sky. A particularly enlightening map of the region and discussion are presented by Herbst and Warner (1981). This complex portion of the sky contains several dark clouds with embedded star-forming regions, the largest of which is the ρ Oph dark cloud, as well as many reflection and emission nebulae, and the diffuse material described in this paper. A *COS B* γ-ray source, CG 353+16, lies in the approximate direction of the ρ Oph cloud and may be the result of shock acceleration of cosmic rays in the cloud (Bignami and Morfill 1980). The path of the runaway star ζ Oph originates in the region of the northern diffuse cloud, the exact location depending on the age of the star; ζ Oph now lies about 15° to the north of the Sco OB2 association (Herbst and Warner 1981). Because of the complexity of the region, it is difficult to assign a single origin for the shock we observed in this program; it is possible that several shocks of different origins exist in the region.

Sancisi (1974) has observed an expanding H I shell centered at galactic coordinates $l = 354°$, $b = +23°$, with a radius of 5°. Sancisi describes the shell as hemispherical, with a radius of 13 pc and a systemic velocity of -1 km s^{-1}, expanding from its center toward the Sco OB2 stars. The center of the shell is near the northern cloud discussed in this paper, and the material in the shell lies between the Sun and the Sco OB2 stars. The southern cloud lines of sight lie about 7° from the northern cloud, so that these stars may be just at the edge of the H I shell. Sancisi (1974) postulated that the shell he observed is a very old supernova remnant. Assuming that the expansion of the shell has been slowed by the dense interstellar medium, he derived an age of 10^6 yr for the remnant. If the path of the runaway star ζ Oph is extrapolated back in time, its position 10^6 years ago is about 2° from the center of the H I shell (Herbst and Warner 1981).

Vrba (1977) has measured the magnetic field direction in the southern ρ Oph cloud. He finds that the magnetic field is aligned with streamers of gas that extend several degrees from the main cloud in the northwest direction. The polarization direction in the main cloud is nearly perpendicular to that in the streamers, leading Vrba (1977) to postulate a shock approaching from the southwest and compressing the most southwesterly material as streamers flow along the magnetic field direction to the northwest. Most star formation should then take place on the southwestern edge of the ρ Oph cloud, which is observed. Vrba (1977) suggests that the origin of shock may be either a galactic spiral density wave or a supernova explosion, although the extent of the shock proposed by him is larger than the H I shell observed by Sancisi (1974). The age of the streamers deduced by Vrba is about 5×10^6 yr, while Sancisi calculated the age of the H I shell as 1×10^6 yr; these values are both approximations, so that the two could be the same age. However, it is difficult to reconcile the geometry of the H I shell with that of the polarization data to infer a single origin for the shock observed here.

In general, our results are consistent with a shock originating in a supernova explosion that generated the H I shell observed by Sancisi (1974). The explosion took place between the Sun and the ρ Oph cloud, and the Sco OB2 stars may have been formed in the dense H I shell. The stars have velocities of 2–3 km s^{-1} away from the Sun relative to the H I shell, which would be expected if the stars were formed earlier in the life of the remnant and retained the velocity of the gas in which they were formed (Sancisi 1974). The velocity of the H I shell, -1 km s^{-1}, agrees with the velocities of the atomic and molecular components assumed here to be postshock gas. The age of the remnant deduced by Sancisi (1974), 10^6 yr, is sufficient for grain enlargement to occur in the postshock gas, as discussed in the previous section.

e) *Other Considerations*

Although a coherent picture of the ρ Oph cloud has been deduced from the data presented in this paper, several problems with this view are also evident. In this section we discuss two considerations that must be included in a complete description of the region. The first is possible contamination of the depletion data by local gas in the lines of sight observed. The second is the observation of Snow and Jenkins (1980) that the depletion pattern is constant for the stars in the ρ Oph cloud.

The local gas has been described by Frisch (1981) and in references cited therein. The solar system appears to be inside a supernova remnant whose center lies 130 pc from the Sun in

the direction of the Scorpius-Ophiuchus region of the sky. The interior gas is manifested in the form of a local interstellar wind, which has a velocity of -25 ± 5 km s^{-1} (heliocentric) from the direction of $\alpha(1950) = 17^h$, $\delta(1950) = -16°$ (approximately 15° to the northeast of the Sco OB2 association). The gas appears to be uniformly less depleted than normal interstellar gas; the increased abundances may be due to processing of the gas through a supernova shock front (Frisch 1981). Since the blueshifted (i.e., preshock) atomic components observed toward the Sco OB2 stars have heliocentric velocities of -13 to -23 km s^{-1}, the projected velocity component of the local wind probably contributes some fraction of the column densities observed for these components. The local neutral material in the Scorpius-Ophiuchus direction has a column density of no more than 5×10^{19} atoms cm^{-2}, deduced from soft X-ray observations (Fried *et al.* 1980). A hydrogen column density of 5×10^{19} cm^{-2} represents between 10% and 50% of the gas in the blueshifted components of the lines of sight observed here, and about 5% of the total line-of-sight column densities.

Using abundances in the line of sight toward α Oph (Frisch 1981), which is 18 pc from the Sun, as typical of the local gas, we have calculated the depletion that would be observed if the local gas contributes a column density of 5×10^{19} cm^{-2} to the blueshifted, preshock atomic components. For example, if we assume that a region containing a column density of 5×10^{19} cm^{-2} of hydrogen toward the ρ Oph stars has a "local" abundance of iron, we can derive an upper limit for the column density of "local" iron. Subtracting the "local" values of N(H I) and N(Fe II) from the measured values for the blueshifted component column densities enables us to calculate upper limits for the preshock gas depletion including the effect of the local gas. (Upper limit here means the largest possible negative number.) Upper limits for iron depletions in the preshock components calculated this way are -1.71, -1.09, -0.56, and -1.73 for β^1, ω^1, σ, and 1 Sco, respectively. For manganese, upper limits on preshock depletions are -0.54, -1.05, and -0.32 for β^1, ω^1, and σ Sco, respectively. In two of the lines of sight, those toward ω^1 Sco and σ Sco, taking the local gas into account actually has the effect of decreasing calculated depletions in the preshock gas. This is because of the generally low total line-of-sight depletions observed in the ρ Oph cloud (e.g., Snow and Jenkins 1980) compared, for example, to the total depletions in the line of sight toward ζ Oph (Snow and Meyers 1979).

There are several reasons why the above upper limits overestimate the effect of the local gas on preshock depletion calculations. The column density of atomic hydrogen toward α Oph is $\leq 4 \times 10^{19}$ cm^{-2} (Frisch 1981), and although all of the gas in the α Oph line of sight is local in some sense, since the star is only 18 pc from the Sun, it is probable that a portion of this gas is not part of the widespread local wind. Observations toward ζ Oph and χ Oph (Frisch 1981) indicate that the column density of local atomic hydrogen toward the ρ Oph cloud is probably $\leq 2 \times 10^{19}$ cm^{-2} rather than 5×10^{19} cm^{-2} as assumed above. In addition, the velocity of the material in the α Oph line of sight ranges in velocity from -20 to -40 km s^{-1} heliocentric (Stokes 1978). In contrast, we have used relatively well-defined velocity components observed by Hobbs (1969, 1971) in H I for our analysis, which further decreases the probable effect of the local gas on calculation of the preshock depletions. Last, the local wind apex is about 15° from the direction of the ρ Oph stars, so that the velocity of the projected component of the gas toward the stars should be ~ -24 km s^{-1} heliocentric. Velocities of the blueshifted components for all the stars observed are ≤ -22 km s^{-1} heliocentric. In the southern region lines of sight (σ Sco and 1 Sco), the preshock component velocities are between -13 and -16 km s^{-1} heliocentric, so that these components should not be significantly contaminated by local gas. In the atomic line profiles for σ Sco and 1 Sco, weak components for which we were not able to calculate depletions were found at more blueshifted velocities (-30 km s^{-1} for σ Sco and -28 km s^{-1} for 1 Sco, both heliocentric). These components, one of which is shown in Figure 1*b*, may arise from local gas contributions. Thus, the effect of the local gas probably does not account for the observed depletion differences between the two main components in the ρ Oph lines of sight, and consideration of the local gas does not affect our conclusion that the postshock gas is more depleted than the preshock gas in the ρ Oph cloud.

The depletion pattern from star to star in the ρ Oph cloud has been observed by Snow and Jenkins (1980), and their observations are difficult to reconcile with the picture of the region developed in this paper. They found that, although total line-of-sight depletions in the ρ Oph cloud vary from star to star, the depletion pattern of the elements is nearly the same for all stars. This observation is consistent with an extended cloud in which most of the depletion originates in a dense core and each line of sight has a different path length through the core portion of the cloud. The observation could also be consistent with grain growth occurring by coagulation rather than by accretion in a shocked gas, since coagulation should not change the overall depletion pattern. In the grain-accretion picture, however, elements that stick more efficiently to grains should be relatively more depleted in lines of sight where the depletion process has gone the furthest, thus changing the overall depletion pattern. Data presented in this paper indicate that there is a well-defined postshock region where some portion of the grain growth occurs by accretion.

It is not known how far the accretion process must proceed in the most depleted postshock gas in order to cause a detectable difference in the patterns of depletion between the most and the least depleted postshock gas. Since the depletion in the ρ Oph cloud is increased only by about a factor of 2 from preshock to postshock gas, it seems unlikely that the different lines of sight observed here would show detectable depletion-pattern differences. While the uncertainties in our data are too large to make an accurate analysis of the depletion patterns in the postshock gas, Table 4 shows that similar depletions for each element exist in all lines of sight observed here. Our observed stars do not include ρ Oph. This star was observed by Snow and Jenkins (1980) and probably has the largest amount of dense material in front of it. While ρ Oph might be expected to show an anomalous depletion pattern, this effect may be washed out in the Snow and Jenkins data by the less depleted local gas and preshock gas.

V. CONCLUSION

We have inferred the presence of a shock wave with a velocity of about 10 km s^{-1} propagating away from the Sun in the direction of the Sco OB2 association. In comparing the preshock and postshock gas, we found that the postshock gas is more depleted than the preshock gas and contains a large molecular component. We conclude that a low-velocity shock, such as the one observed here, enhances grain growth in the shocked interstellar gas. The grain growth may occur through

some combination of accretion and coagulation, resulting in a grain distribution in which there is an excess of large grains and a deficiency of very small grains. The resultant grain distribution is consistent with anomalous extinction curves previously observed for the ρ Oph cloud. Our conclusion is also consistent with theoretical work on grain-destruction mechanisms; no mechanisms proposed for grain destruction in shock waves (e.g., Barlow and Silk 1977; Shull 1978; Cowie 1978; Draine and Salpeter 1979; Havnes 1980) predict destruction at velocities $\lesssim 30\ \mathrm{km\ s^{-1}}$.

The gas that we have observed is part of a complex, active region of the sky. We have attempted to isolate one of the many phenomena now occurring in the ρ Oph cloud. Because of the uncertainties involved, and because these observations are the first to examine in detail the effects of a low-velocity shock on the interstellar medium, our conclusions must be somewhat tentative. Further observations of lines of sight that are likely to contain a low-velocity shock (see, e.g., Federman 1982*a*, *b*) are needed to confirm the effects described in this paper.

This research has been supported by National Aeronautics and Space Administration grants NS6-7626 and NA65-15 with the University of Colorado. S. R. F. acknowledges grant F-623 of the Robert A. Welch Foundation. Helpful discussions with Dr. J. M. Shull are gratefully acknowledged. We thank an anonymous referee for helpful comments.

REFERENCES

Barlow, M. J., and Silk, J. 1977, *Ap. J.*, **229**, 545.
Bignami, G. F., and Morfill, G. E. 1980, *Astr. Ap.*, **87**, 85.
Bless, R. C., and Savage, B. D. 1972, *Ap. J.*, **171**, 293.
Bohlin, R. C., Hill, J. K., Jenkins, E. B., Savage, B. D., Snow, T. P., Spitzer, L., and York, D. G., 1983, *Ap. J. Suppl*, **51**, 277.
Bohlin, R. C., Savage, B. D., and Drake, J. F. 1978, *Ap. J.*, **224**, 132.
Breger, M. 1979, *Ap. J.*, **204**, 789.
Bronfman, L. 1980, M.S. thesis, University of Chile.
Carrasco, L., Strom, S. E., and Strom, K. M. 1973, *Ap. J.*, **182**, 95.
Cowie, L. L. 1978, *Ap. J.*, **226**, 858.
Crutcher, R. M. 1976, *Ap. J.*, **208**, 382.
Draine, B. T., and Salpeter, E. E. 1979, *Ap. J.*, **231**, 77.
Dyson, J. E., and Williams, D. A. 1980, *The Physics of the Interstellar Medium* (New York: Wiley).
Elitzur, M., and Watson, W. D. 1978, *Ap. J. (Letters)*, **222**, L14.
———. 1980, *Ap. J.*, **236**, 172.
Federman, S. R. 1980, *Ap. J. (Letters)*, **241**, L109.
———. 1981, *Astr. Ap.*, **96**, 198.
———. 1982*a*, *Ap. J.*, **253**, 601.
———. 1982*b*, *Ap. J.*, **257**, 125.
Field, G. B. 1974, *Ap. J.*, **187**, 453.
Freid, P. M., Nousek, J. A., Sanders, W. T., and Kraushaar, W. L. 1980, *Ap. J.*, **242**, 987.
Frisch, P. C. 1979, *Ap. J.*, **227**, 474.
———. 1981, *Nature*, **293**, 377.
Havnes, O. 1980, *Astr. Ap.*, **90**, 106.
Herbst, W., and Warner, J. W. 1981, *A.J.*, **86**, 885.
Hobbs, L. M. 1969, *Ap. J.*, **157**, 135.
———. 1971, *Ap. J.*, **166**, 333.
———. 1973, *Ap. J.*, **181**, 79.
Jura, M. 1980, *Ap. J.*, **222**, 863.
Liszt, H. 1981, *Ap. J. (Letters)*, **246**, L147.
Marschall, L. A., and Hobbs, L. M. 1972, *Ap. J.*, **173**, 43.
Morton, D. C. 1978, *Ap. J.*, **222**, 863.
Morton, D. C., and Smith, W. H. 1973, *Ap. J. Suppl.*, **26**, 333.
Olthof, H. and Pottasch, S. R. 1975, *Astr. Ap.*, **43**, 291.
Rogerson, J. B., Spitzer, L., Drake, J. F., Dressler, K., Jenkins, E. B. Morton, D. C., and York, D. G. 1973, *Ap. J. (Letters)*, **181**, L97.
Routly, P. M., and Spitzer, L. 1952, *Ap. J.*, **115**, 227.
Sancisi, R. 1974, *IAU Symposium 60, Galactic Radio Astronomy*, ed. F. J. Kerr and S. C. Simonson (Dordrecht: Reidel), p. 115.
Savage, B. D., and Bohlin, R. C. 1979, *Ap. J.*, **229**, 136.
Savage, B. D., Bohlin, R. C., Drake, J. F., and Budich, W. 1977, *Ap. J.*, **216**, 291.
Seab, C. G., and Shull, J. M. 1983, *Ap. J.*, **275**, 652.
Seab, C. G., Snow, T. P., and Joseph, C. L. 1981, *Ap. J.*, **246**, 788.
Serkowski, K., Mathewson, D. S., and Ford, V. L. 1975, *Ap. J.*, **196**, 261 (SMF).
Shull, J. M. 1978, *Ap. J.*, **226**, 858.
Shull, J. M., and York, D. G. 1977, *Ap. J.*, **211**, 803.
Shull, J. M., York, D. G., and Hobbs, L. M. 1977, *Ap. J. (Letters)*, **211**, L139.
Siluk, R. S., and Silk, J. 1974, *Ap. J.*, **192**, 51.
Snow, T. P. 1975, *Ap. J. (Letters)*, **202**, L87.
Snow, T. P., and Jenkins, E. B. 1980, *Ap. J.*, **241**, 161.
Snow, T. P., and Meyers, K. A. 1979, *Ap. J.*, **229**, 545.
Snow, T. P., and York, D. G. 1975, *Ap. Space Sci.*, **34**, 19.
Spitzer, L. 1976, *Comm. Ap.*, **6**, 177.
———. 1978, *Physical Processes in the Interstellar Medium* (New York: Wiley), pp. 191–213.
Spitzer, L., Cochran, W. D., and Hirshfield, A. 1974, *Ap. J. Suppl.*, **28**, 373.
Stokes, G. M. 1978, *Ap. J. Suppl.*, **36**, 115.
Stokes, G. M., and Hobbs, L. M. 1976, *Ap. J. (Letters)*, **208**, L95.
Vogt, S. S., Tull, R. G., and Kelton, P. 1978, *Appl. Optics*, **17**, 574.
Vrba, F. J. 1977, *A.J.*, **82**, 198.
Withbroe, G. D. 1971, *The Menzel Symposium*, ed. K. B. Gebbie (NBS Spec. Pub. 353; Washington: GPO).
York, D. G., and Miller, A. E. 1974, Memo to Users of Copernicus Data, December 9.

M. Breger: Vienna University Observatory, Astronomisches Institut, Turkenschanzstrasse 17, A-1180 Vienna, Austria

S. R. Federman: 183–601, Jet Propulsion Laboratory, 4800 Oak Grove Drive, Pasadena, CA 91109

K. A. Meyers: Department of Astronomy, Ohio State University, 174 West 18th Avenue, Columbus, OH 43210

T. P. Snow: Laboratory for Atmospheric and Space Physics, University of Colorado, Boulder, CO 80309